Materials Letters 128 (2014) 199–203

Contents lists available at ScienceDirect

Materials Letters

journal homepage: www.elsevier.com/locate/matlet

Effect of rare earth additions on the critical resolved shear stresses of magnesium alloys

V. Herrera-Solaz [a], P. Hidalgo-Manrique [b], M.T. Pérez-Prado [b], D. Letzig [c], J. Llorca [a,b], J. Segurado [a,b,*]

[a] Department of Materials Science, Polytechnic University of Madrid, E. T. S. de Ingenieros de Caminos, 28040 Madrid, Spain
[b] IMDEA Materials Institute, C/Eric Kandel 2, 2890 Getafe, Madrid, Spain
[c] Magnesium Innovation Centre MagIC, Helmholtz-Zentrum Geesthacht, Max-Planck-Strasse 1, D-21502 Geesthacht, Germany

ARTICLE INFO

Article history:
Received 8 April 2014
Accepted 22 April 2014
Available online 30 April 2014

Keywords:
Critical resolved shear stresses
Crystal plasticity
Rare earths
Magnesium alloys
Inverse optimization

ABSTRACT

An inverse optimization strategy based on crystal plasticity finite element simulations of polycrystals was used to obtain the critical resolved shear stresses of two Mg–1%Mn alloys containing neodymium from macroscopic experimental data. It was found that, with respect to pure Mg, the presence of Nd increases the $CRSS_{basal}$, $CRSS_{twinning}$, and the $CRSS_{basal}/CRSS_{twinning}$ ratio and decreases the $CRSS_{non\text{-}basal}/CRSS_{twinning}$ ratio. Additions of neodymium as high as 1 wt% result in similar CRSSs values for all deformation modes and, thus, in an isotropic yielding behavior.

Magnesium (Mg) alloys deform by crystallographic slip along certain directions on basal, prismatic and pyramidal planes and by mechanical twinning [1]. The ease of activation of each deformation mechanism is related to the corresponding critical resolved shear stress (CRSS). It is generally accepted that $CRSS_{basal} < CRSS_{twinning} < CRSS_{prismatic} < CRSS_{pyramidal}$ at low temperatures [2]. Moreover, the relative activity of each deformation mechanism is highly dependent on texture due to the small number of independent slip systems [3]. This anisotropy is further accentuated by the polar nature of twinning [4] which, for a given texture, may lead to different activities of the available deformation systems in tension and compression, giving rise to a yield asymmetry [5]. Wrought Mg alloys exhibit a particularly pronounced yield stress anisotropy and asymmetry at room temperature (RT) due to their sharp crystallographic textures [6]. This behavior hinders their use to a large extent, in spite of their potential for lightweight structural elements [7].

It has recently been shown that alloying with certain rare-earth (RE) elements might lead to a complete elimination of the RT yield anisotropy and asymmetry in wrought Mg alloys [8–12]. RE additions influence dynamic recrystallization during processing and lead to weak deformation textures [8–10]. However, some studies [11,12] suggest that such weak textures alone cannot explain the isotropic mechanical behavior and that changes in the CRSSs of the different deformation modes with respect to non-RE Mg alloys must also concur. These changes have not been quantified to date and the origin of the influence of the RE elements on the CRSS values for Mg alloys is currently not fully understood.

In this work, the values of CRSSs of the extruded alloys Mg–1% Mn–0.5 wt%Nd (MN10) and Mg–1%Mn–1 wt%Nd (MN11) are obtained by an inverse optimization strategy [14] from the experimental stress–strain curves of uniaxial tests along different orientations with respect to the extrusion axis (ED). The optimization method is based on computational homogenization of the polycrystal behavior by means of crystal plasticity finite element (CPFE) simulations of a representative volume element (RVE) of the microstructure. The result of the optimization is the set of CRSSs that lead to the best agreement between experimental results and the corresponding numerical simulations. Thus, the effect of Nd on the CRSSs can be quantified by comparing the values obtained for MN10 and MN11 Mg alloys with those corresponding to pure Mg.

The MN10 and MN11 alloys were gravity cast to produce billets for extrusion with a diameter of 93 mm. The billets were homogenized at 350 °C during 15 h before processing. Then, indirect extrusion of MN10 and MN11 billets was carried out at 360 °C and 350 °C, respectively, at 2.8 mm/s, to produce round bars of 17 mm in diameter (extrusion ratio equal to 1:30), which were subsequently air-cooled. Uniaxial tension and compression tests were

* Corresponding author at: Department of Materials Science, Polytechnic University of Madrid, E. T. S. de Ingenieros de Caminos. 28040 Madrid, Spain. Tel.: +34 91 3365246; fax: +34 91 3366680.
E-mail address: jsegurado@mater.upm.es (J. Segurado).

http://dx.doi.org/10.1016/j.matlet.2014.04.144
0167-577X/

performed on the as-extruded bars at RT and at an initial strain rate of $10^{-3}\,s^{-1}$ using an Instron universal testing machine. Dog-bone tensile specimens, with gauge dimensions of 4 mm in diameter and 12 mm in length, were machined with their loading axis parallel to the extrusion direction (ED). The compressive specimens were cylinders with 3 mm in diameter and 4.5 mm in length machined with their loading axis parallel to the ED, inclined 45° towards the ED and perpendicular to the ED. The microstructure was studied by optical microscopy (OM) in an Olympus BX-51 microscope. The metallographic preparation consisted of several grinding and polishing steps followed by chemical etching in a solution based on picric and acetic acids in order to reveal grain boundaries. The macrotexture was measured by X-ray diffraction (XRD). The (0001), $(10\bar{1}0)$, $(10\bar{1}1)$, $(10\bar{1}2)$, $(10\bar{1}3)$ and $(10\bar{1}0)$ pole figures were measured using Cu Kα radiation in a XPert PRO ALPHA1 PANalytical diffractometer furnished with a PW3050/60 goniometer. From these experimental data, the ODF and the pole figures were obtained using the MATLAB toolbox MTEX [15]. The inverse pole figures were then derived from the direct pole figures.

The effective behavior of MN10 and MN11 Mg alloys was determined through the CPFE simulation of an RVE of the polycrystalline microstructure. The crystal plasticity model of each grain is presented in detail in [14] and accounts for the dominant deformation modes of Mg alloys: basal $\langle a\rangle$, prismatic $\langle a\rangle$ and pyramidal $\langle c+a\rangle$ slip as well as tensile twinning. Each slip and twinning mode is characterized by a CRSS function that evolves with accumulated shear strain on the different systems. The shape of this function for each deformation mode is defined using three parameters, namely the initial and saturation CRSSs (τ_0, τ_s) and the initial hardening modulus h_0.

The polycrystalline RVEs are cubic volumes discretized with cubic finite elements [16]. RVEs with different levels of complexity were used: from simple RVEs where each cubic element represents a grain (125, 512 and 1000 crystals per RVE were used) to complex RVEs which provide a realistic representation of the grain size and shape within the polycrystal. The RVEs for these latter models were generated using Dream3D [17]. An equiaxed grain shape was chosen and the grain size distribution followed a log-norm function. The realistic models included 300 grains with approximately 200 voxel elements per grain (Fig. 1). The grain orientations in all RVEs were determined from the experimental orientation distribution function (ODF) of the initial texture. The orientation of each grain was obtained by a Monte Carlo lottery and the larger the number of grains, the higher the accuracy in the model texture.

The mechanical behavior of the polycrystalline RVE under a given deformation history was obtained by the finite element method using periodic boundary conditions. The single crystal behavior is dictated by a set of parameters $\boldsymbol{\beta}$, which defines the evolution of the CRSS of the slip and twinning modes considered (τ_0, τ_s and h_0 for each deformation mode). An objective error function $O(\boldsymbol{\beta})$ can be built from the experimental stress–strain curves and the corresponding numerical simulations according to

$$O(\beta) = \sum_{i=1}^{n} |y_i - f(x_i, \beta)|$$

where (x_i, y_i) stands for a set of n points defining the experimental stress–strain curves and $(x_i, f(x_i, \boldsymbol{\beta}))$ are the corresponding points obtained by computational homogenization. An inverse optimization strategy based on the Levenberg–Marquardt method was used to find the set of parameters $\boldsymbol{\beta}$ that minimizes the objective error function $O(\boldsymbol{\beta})$ [14]. The optimization procedure is highly non-linear and began using a simple RVE in which each grain is represented by one voxel. The number of crystals in the RVE increased progressively (125, 512 and 1000) once the optimization algorithm has reached the optimum solution for each RVE. Final optimization was carried out with the complex RVE in Fig. 1. This hierarchical strategy was very efficient and reduced considerably the computational resources necessary to carry out the optimization.

The as-extruded MN10 and MN11 round bars were fully recrystallized and their microstructure was formed by equiaxed grains with average diameters of 21 μm and 17 μm, respectively. The initial texture of both alloys, measured at the center of the bars, is shown in Fig. 2 by means of inverse pole figures. Both textures are weaker than those typical of extruded non-RE containing Mg alloys [6]. The weak texture is especially pronounced in the MN11 bar while a slight tendency for the ED to be aligned in the $\langle 10\bar{1}0\rangle$ direction is still observed in the MN10 bar. The origin of this weak texture is still under debate. It has been proposed that, in RE-containing alloys, there is a larger tendency for recrystallized grains to nucleate at shear bands and that the orientations of such nuclei become more widely spread as the Nd content increases [13]. It has also been suggested that the presence of RE solutes and intermetallic particles hinder the grain boundary mobility, thereby delaying the preferred growth of certain

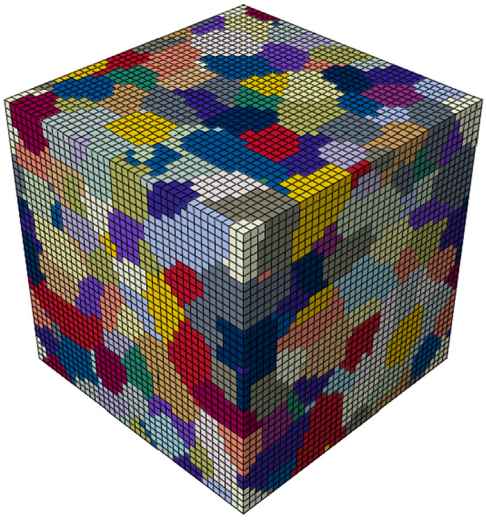

Fig. 1. Cubic RVE of the microstructure including 300 crystals discretized with 200 cubic finite elements per grain.

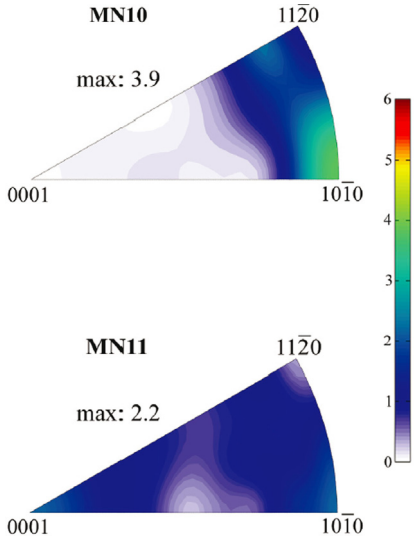

Fig. 2. Inverse pole figures showing the orientation of the extrusion direction of the (a) MN10 and (b) MN11 alloys in the as-extruded condition.